RSC Advances

ROYAL SOCIETY OF CHEMISTRY

www.rsc.org/advances

Cite this: DOI: 10.1039/c0xx00000x

www.rsc.org/xxxxxx

ARTICLE TYPE

Electrochemical fabrication of hydrangea macrophylla flower-like Pt hierarchical nanostructures and their properties for methanol electrooxidation

Xia Wang, Yue Sun, Jun Hu, Yong-Jun Li* and Edward S. Yeung

Received (in XXX, XXX) Xth XXXXXXXXX 20XX, Accepted Xth XXXXXXXXX 20XX
DOI: 10.1039/b000000x

Electrochemical preparation of non-carbon supported catalysts is a favourable way for fuel cells to keep catalysts from agglomeration during the electrocatalytic process and provide the catalyst layer with higher mechanical stability than the established drop-coating deposition of a mixture of catalysts and carbon powder. Here, one-step current-directed approach is proposed to fabricate 3-dimensional (3D) Pt hierarchical nanostructures (3DPHNs) without any capping agents. The resulting 3DPHNs were composed of hydrangea macrophylla flower-like Pt microspheres, and each microsphere consisted of many nano-petals. The size, the number density and the exposed facets of Pt microspheres in 3DPHNs can be adjusted by changing the current density of Pt deposition. High-resolution transmission electron microscopy (HRTEM) revealed that Pt nano-petals obtained at deposition current densities higher or lower than 3.5 mA/cm^2 contained Pt{200} and Pt{111} facets. However, Pt nano-petals obtained at 3.5 mA/cm^2 were single crystals with {111} orientation that showed better specific catalytic activity and stability to methanol electrooxidation compared to commercial Pt/C catalyst due to its resistance to catalyst agglomeration, the exposure of specific facets and the specific nanostructure.

1 Introduction

Platinum always attracts particular attention of scientists due to its broad catalytic applications in organic reactions[1] and cleaning of exhaust gas[2] and fuel cells.[3,4] Although Pt is an indispensable metal in the catalytic field, its reserves on earth are very limited and Pt catalyst is apt to be poisoned by CO-like intermediates. To maintain sustainable development, Pt-based catalysts have been widely studied, such as binary and ternary alloys[3,5] and core-shell structures.[6-8] Studies have demonstrated[9,10] that Pt electrocatalytic activity (EA) or tolerance towards CO-like poisoning molecules can be enhanced through the synergistic effect between Pt and other metallic elements such as Au,[11] Cu[12] or Pb,[13] which is a significant alternative to solve the problems caused by pure Pt catalysts. However, to effectively design binary or ternary metal catalysts, it is essential to first improve our understanding of the catalytic mechanism of pure Pt metal.

The catalytic performance of Pt is mainly dependent on two aspects: Pt particle size and shape. To date, the effect of particle size has been well elucidated: Pt particles less than 10 nm were preferable. To conveniently manipulate catalysts and effectively exploit Pt atoms, commercial Pt catalyst particles usually were ~ 3 nm. Surfaces of spherical Pt nanoparticles commonly consisted of mixed crystallographic facets, such as {111}, {100} and {110} facets.[14] Different facets have different catalytic effects on specified reactions.[15] Methanol electrooxidation on platinum takes place in acidic electrolytes involving the following adsorbed intermediates, such as CO_{ads}, $HCOO_{ads}$, formaldehyde and formic acid.[16-18] CO_{ads} has been identified as a key poisoning molecule in the process of methanol oxidation. CO_{ads} molecules absorbed on Pt{100} and Pt{111} were considered to be produced by an indirect and direct pathway, respectively.[16,19] Thus, Pt{111} facets were expected to facilitate the methanol oxidation via the direct pathway and exhibited a good tolerance to CO poisoning.[16]

To efficiently improve Pt catalytic activity, specific facets of Pt are exposed by optimizing the synthetic method so that Pt particles exhibit a certain shape in appearance. All kinds of shapes were also successfully synthesized in solution by reducing Pt precursors, such as Pt polyhedral,[20] nanowires[21], nanorods,[22] nanotubes,[23] nanocubes,[24,25] nanosheets,[26] fivefold stars[27] and flower-like nanostructures.[28] Pt concave nanocubes exhibited 2.5 times better specific electrocatalytic activity than Pt/C catalysts for formic acid electrooxidation.[25] Compared with the wet-chemical synthesis mentioned above, electrochemical preparation is a much easier and faster protocol and the final morphology and size of electrodeposited target materials can be controlled simply by varying the applied potential, the current density, the type of the electrochemical technique, precursor concentration, pH value or electrodeposition time.[29] To date Pt nanostructures with a variety of shapes have been electrochemically synthesized, such as cubic nanobox,[30] nanowire array,[31] cauliflower-like,[32] needle-like,[32] honeycomb[33] and nanosheet,[34] and these unusually shaped Pt nanostructures exhibited better catalytic activity towards alcohol oxidation.[35] For example, tetrahexahedral Pt nanocrystals

bound by high-index facets {730} were first electrochemically prepared by the combination of Sun's group and Wang's group,[36] and showed excellent catalytic activities: 2 times and 3.3 times that of commercial Pt/C catalysts towards electrooxidation of formic acid and ethanol, respectively. The shape control was achieved mainly by the template-directed growth[31] or potential-interfered growth (e.g. potentiostatic method,[38] pulse electrodeposition,[37] square wave voltammetry[36] and staircase voltammetry[32]). One-step current-directed growth methods were rarely used for the production of shaped Pt nanostructure to the best of our knowledge.[39,40]

Herein, a one-step current-directed approach is proposed to fabricate capping-agent-free three-dimensional Pt hierarchical structure (3DPHN) composed of hydrangea macrophylla flower-like Pt microspheres, and each sphere consisted of many entangled nano-petals. Also, the number density and exposed facets of nano-petals on the electrode substrate could be adjusted by changing the magnitude of the applied current. The optimized 3DPHN showed better electrocatalytic activity (EA) and stability towards methanol oxidation than commercial Pt/C catalyst.

2 Materials and methods

2.1 Chemicals

Potassium hexachloroplatinate (VI) (K_2PtCl_6, ≥ 99.79%), perchloric acid ($HClO_4$, ≥ 72.0%), methanol (CH_3OH, ≥ 99.5%), and sulfuric acid (H_2SO_4, 95%~98%) were supplied by Shanghai Chemical Reagent Company (China). Pt/C (20 wt% Pt) commercial catalyst was purchased from Johnson Matthey Company. Milli-Q water was used in all experiments.

2.2 Electrochemical preparation of three-dimensional Pt hierarchical nanostructures (3DPHNs)

Electrodeposition was conducted on a homemade inverted three-electrode cell. The so-called 'inverted' means that the working electrode (glassy carbon, GC, 3 mm in diameter), was put into the cell from the bottom, which was at the same level as the bottom of the cell. A saturated calomel electrode (SCE) and a platinum wire were used as the reference electrode and the counter electrode, respectively. All potentials mentioned below were referred to SCE unless otherwise specified.

Before electrodeposition, the GC disc surface was polished successively with 1.0 μm-, 0.3 μm- and 0.05 μm-alumina slurry, and then ultrasonically rinsed twice with copious amounts of water and ethanol. The freshly cleaned GC electrode was used for Pt electrodeposition in 50 mL of aqueous solution containing 2.0 mmol/L K_2PtCl_6 and 1.0 mol/L $HClO_4$. The electrodeposition was carried out galvanostatically at room temperature and the applied cathodic current densities ranged from 0.14 mA/cm^2 to 7.0 mA/cm^2. The deposition time was 40 min. After electrodeposition was completed, as-prepared Pt nanostructures were rinsed with water for characterization and methanol electrooxidation.

2.3 Methanol electrooxidation

Methanol electrooxidation was conducted in a conventional three-electrode configuration. The working electrode was a GC disc covered with Pt nanostructure (GC/Pt), which was further cleaned before electrooxidizing methanol by cycling potentials from – 0.25 V to 1.2 V in 0.5 mol/L H_2SO_4 aqueous solution until the potential-current pattern remained unchanged. Measurement of methanol electrooxidation was carried out in 50 mL of 0.5 mol/L H_2SO_4 + 1.0 mol/L CH_3OH solution that was aerated with N_2 for 15 min to eliminate dissolved O_2 before measurement. For comparison, the commercial Pt/C electrode was prepared as well: 1.0 mL of 0.05 wt% Nafion ethanol solution containing 5 mg of Pt/C was pipetted onto a GC disc (diameter, 3 mm) and dried at room temperature.

2.4 Characterization

All electrochemical experiments were performed using a CHI 660D workstation (Chenhua, Shanghai). Scanning electron microscopic (SEM) images were taken on a scanning electron microscope (Hitachi-S4800) operating at 10 kV. Energy dispersive X-ray spectrometer (EDS) and high resolution transmission electron microscopy (HRTEM) was performed on a T20 (EEI, America) microscope with an accelerating voltage of 200 kV.

3 Results and discussion

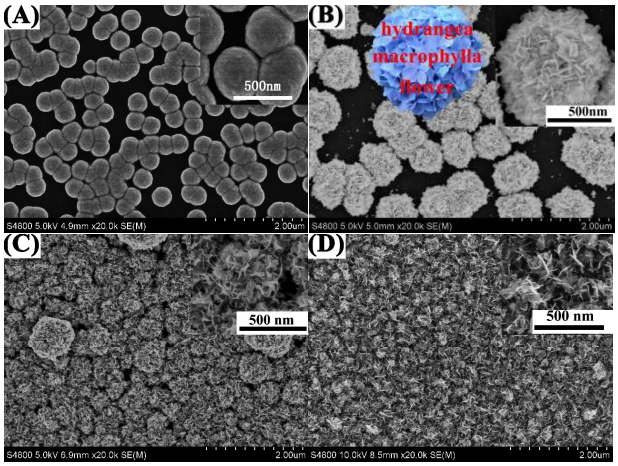

Figure 1 SEM images of 3D Pt hierarchical nanostructures at different cathodic current densities: (A) 0.14 mA/cm^2, (B) 0.7 mA/cm^2, (C) 3.5 mA/cm^2, and (D) 7.0 mA/cm^2. The electrodeposition time was 40 min. Grey insets were SEM images with higher magnification; colorful inset in Figure 1B was the digital image of a hydrangea macrophylla flower.

The current density of electrodeposition has a critical influence on the morphologies of the resultant Pt nanostructures. When the current density was 0.14 mA/cm^2, as-prepared 3D Pt nanostructure was composed of inter-connected Pt solid spheres, and these spheres had a large size ranging from 260 nm to 470 nm (Figure 1A). Large Pt solid spheres are not sustainable for catalytic reactions because of their limited surface areas. However, when the current density was 0.7 mA/cm^2, larger Pt spheres were produced with a diameter ranging from 460 nm to 920 nm (Figure 1B). Interestingly, these larger Pt spheres had hierarchical structures composed of many nano-petals, just like hydrangea macrophylla flowers (colorful inset in Figure 1B). The average thickness of nano-pedals was about 10 nm according to the estimation from SEM images with a high magnification (inset

in Figure 1B). With the increase of the current density from 0.7 mA/cm^2 to 3.5 mA/cm^2 and then to 7.0 mA/cm^2, all resultant Pt nanostructures were constructed by Pt nano-petals (Figure 1C and D). The only difference was the number density of Pt nano-petals on GC surface. At 3.5 mA/cm^2, the whole GC surface was covered with inter-connected Pt hierarchical spheres, the outline of which was distinguishable, and some Pt hierarchical spheres were sparsely decorated on the top of the Pt nanostructure, forming the-second-layer-Pt nanostructure. At 7.0 mA/cm^2, what we observed was 3D dense nano-petal structure and single Pt hierarchical spheres were nearly undistinguishable.

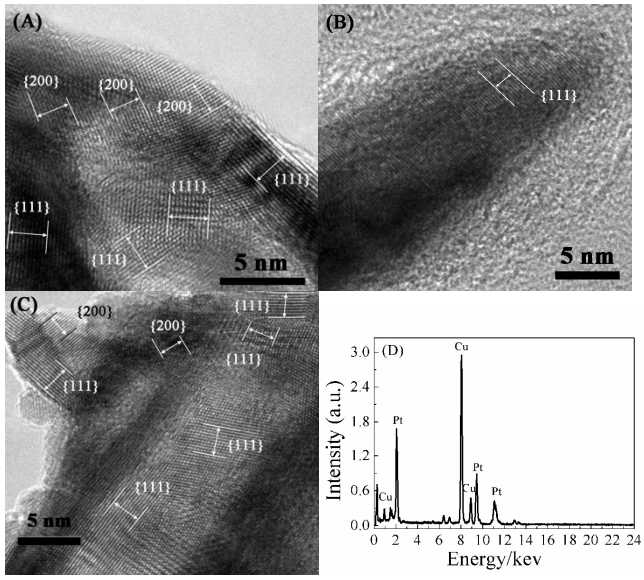

Figure 2 Representative HRTEM images of 3DPHNs obtained at different current densities: (A) 0.7 mA/cm^2, (B) 3.5 mA/cm^2, and (C) 7.0 mA/cm^2. (D) EDS pattern of 3DPHNs.

HRTEM images (Figure 2A and C) reveal that the inter-fringe distances of Pt nano-petals prepared at the 0.7 mA/cm^2 and 7.0 mA/cm^2 were ~ 0.224 nm and ~ 0.199 nm, respectively, which were ascribed to the lattice spacing of the Pt{111} and Pt{200} planes. However, as for Pt nano-petals obtained at 3.5 mA/cm^2 (Figure 2B), the inter-fringe distance of the whole Pt nano-petal was ~ 0.224 nm, indicating that they grew along the Pt{111} plane direction. All EDS patterns of hydrangea macrophylla flower-like Pt nanostructures were the same, as shown in Figure 2D, which exhibited the characteristic peaks of Cu and Pt. Regardless of the copper and carbon coming from the substrate, Cu grid and the carbon film, only Pt peaks remained, i.e. the resultant 3DPHNs were pure Pt.

Current density is crucial to the crystallization of Pt in the process of electrodeposition. At the current density of 3.5 mA/cm^2, only Pt{111} facets were detected, indicating that Pt nano-pedals grew exclusively along the {111} direction, which was attributed to the effect of the surface energy of crystal faces.[41] Generally, the facets with the low surface energy are easily formed during the growth of a crystal. Although the surface energy of the crystal facets depends on the intrinsic properties of materials, it can be remarkably lowered by surface adsorption.[42] In our case, the growth of Pt nano-pedals exclusively along the {111} direction may be closely linked with the surface adsorption of H ions on other facets of Pt. By adjusting the current density of deposition to control surface adsorption of H ions, single-crystal Ni, ZnS and CdS nanowires have been successfully produced.[41,43] On the other hand, a suitable current density was able to ensure $PtCl_6^{2-}$ ions to arrive at the electrode from the electrolyte to find thermodynamically favorable locations to attach and grow along {111} orientation. Shen et al.[40] also found that Pt single crystal nanoparticles were obtained only at a medium current density. Either too high or too low current densities only produced multi-crystalline Pt nanoparticles.

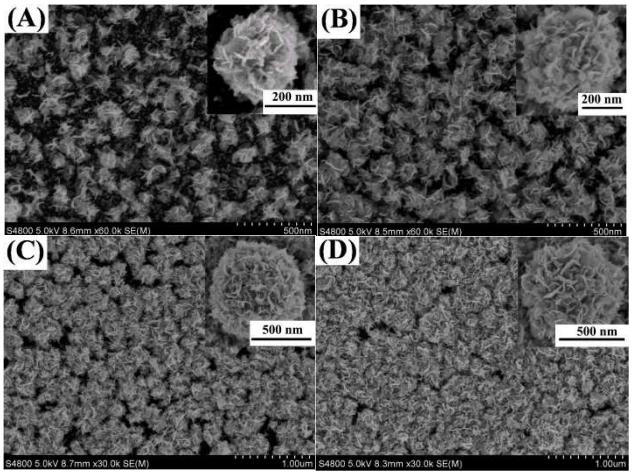

Figure 3 SEM images of 3D Pt hierarchical nanostructures obtained with the cathodic current density of 3.5 mA/cm^2 at different growth stages: (A) 5 min, (B) 10 min, (C) 15 min, and (D) 30 min. Insets were SEM images with higher magnification.

To understand the formation mechanism of Pt hierarchical spheres, we tracked the growth process of 3DPHN obtained at 3.5 mA/cm^2, as shown in Figure 3. When the deposition time (t) increased from 5 min to 40 min (Figure 1 and Figure 3), we observed the number density of Pt hierarchical spheres rose. At deposition time t = 5 min, sparse Pt hierarchical spheres (diameter, ~ 100 nm) distributed over the entire GC surface (Figure 3A). On close inspection of the SEM image, ~ 14-nm Pt nanoparticles were observed in the gaps among Pt hierarchical spheres, suggesting that Pt hierarchical spheres were formed with these small Pt nanoparticles as nucleation centers. With the increase of the deposition time to 10 min, each Pt hierarchical sphere further grew along the three dimensional directions and had a diameter of ~ 140 nm. The gaps between Pt hierarchical spheres reduced. As the electrodeposition time continued to increase from 10 min to 15 min, the size of 3DPHNs increased from ~ 140 nm to ~ 240 nm and the gaps between Pt hierarchical spheres further decreased. At the same time, the diameter of 3DPHNs increased from ~ 500 nm to ~ 690 nm. When the deposition time reached 30 min, the morphology of Pt hierarchical structure (Figure 3D) was similar to that produced after 40-min electrodeposition (Figure 1D), but the difference is that 40-min electrodeposition continued to create a second-layer Pt hierarchical spheres, as observed in Figure 1D.

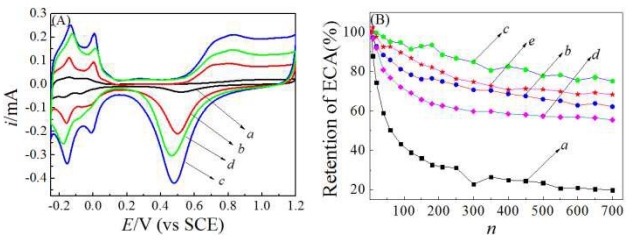

Figure 4 (A) Cyclic voltammograms for 3DPHNs in deoxygenated 0.5 mol/L H_2SO_4 solution. The scan rate is 50 mV/s. (B) The relationship between the retention of ECAs and cycle number, *n*. The current density of deposition: (*a*) 0.14 mA/cm^2, (*b*) 0.7 mA/cm^2, (*c*) 3.5 mA/cm^2, (*d*) 7.0 mA/cm^2 and (*e*) Pt/C.

All the nanostructures obtained at different current densities showed the characteristic peaks of Pt metal when they were cycled in H_2SO_4 solution from – 0.25 V to 1.20 V (Figure 4A): hydrogen adsorption/desorption peaks at the range between – 0.25 V and 0.05 V, oxidation peaks of Pt (~ 0.8 V) at the positive-going segments, and reduction peaks of Pt oxides (~ 0.48 V) at the negative-going segments. Additionally, the major differences for cyclic voltammograms of the different samples were the magnitude of hydrogen adsorption/desorption peak current, which was well-known to be closely linked with the electrochemical active area (ECA) of the Pt nanostructure. The larger the ECA, the larger was the magnitude of hydrogen adsorption/desorption peak current. This trend was consistent with that of the reduction peak current of platinum oxide at ~ 0.48 V. Structural stabilities of 3DPHNs obtained at different current densities were evaluated by considering the retention of ECAs under continuous cycling from – 0.25 V to 1.0 V in H_2SO_4, as shown in Figure 4B. ECAs were calculated by integrating the charge of the hydrogen adsorption/desorption peaks.[44] Among all samples, 3DPHNs obtained at a current density of 0.14 mA/cm^2 had the worse stability and the ECA declined rapidly to ~ 20 % of the initial value after 700 cycles (9.7 h). Other samples were relatively stable, and the retention of ECAs was more than 55% after 700 cycles. The 3DPHNs obtained at a current density of 3.5 mA/cm^2 exhibited the best mechanical stability: ~ 75% of ECA was maintained after 700 cycles, which was larger than that of the commercial Pt/C catalyst (68% retention) (Figure 4B curve *e*).

To better understand the relation between the electrocatalytic activity (EA) and Pt nanostructures, all as-prepared 3DPHNs and commercial Pt/C were used to electrocatalyze methanol oxidation, as shown in Figure 5A. All catalytic currents were normalized to ECAs. In the positive-going direction, oxidation peaks appeared in the potential range from 0.61 V to 0.68 V due to methanol oxidation.[35] The difference of peak potentials may be attributed to the fine difference of Pt nanostructures.[45] With the increase of current densities of Pt deposition from 0.14 mA/cm^2 to 3.5 mA/cm^2, the current densities of methanol oxidation peaks increased and reached up to the maximum value at 3.5 mA/cm^2, which is slightly higher than that of commercial Pt/C. However, when the deposition current density further increased to 7.0 mA/cm^2, the oxidation peak current density declined. In the negative-going direction, another oxidation peak appeared in the range from 0.47 V to 0.51 V, which was attributed to the oxidations of adsorbed CO or CO-like species.[46] The cyclic voltammetric study indicated that 3DPHN prepared at 3.5 mA/cm^2 had the best specific EA and better than the Pt/C commercial catalyst, similar to the Pt dendritic hierarchical nanostructures reported before.[47]

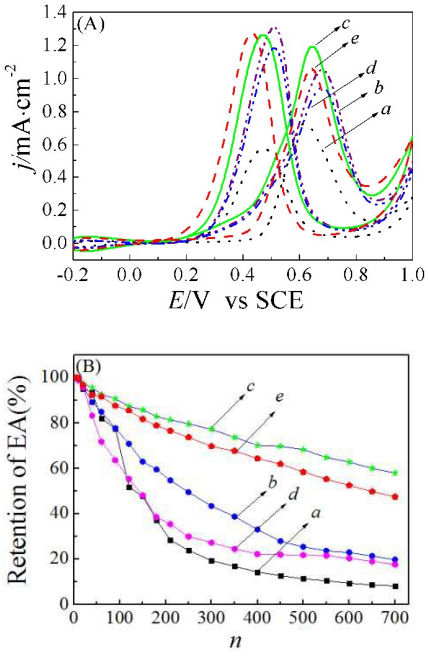

Figure 5 (A) Cyclic voltammograms for 3DPHNs in nitrogen-saturated 1.0 mol/L CH_3OH + 0.5 mol/L H_2SO_4 solution. The scan rate is 50 mV/s. (B) The relationship between the retention of EAs and cycle number, *n*. The current densities of deposition: (*a*) 0.14 mA/cm^2, (*b*) 0.7 mA/cm^2, (*c*) 3.5 mA/cm^2, (*d*) 7.0 mA/cm^2 and (*e*) Pt/C.

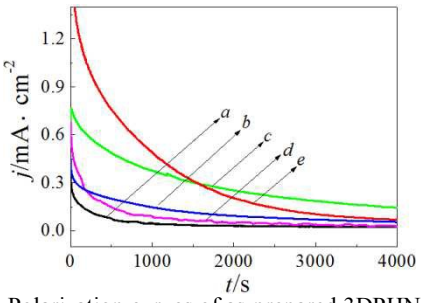

Figure 6 Polarization curves of as-prepared 3DPHNs in nitrogen-saturated 1.0 mol/L CH_3OH + 0.5 mol/L H_2SO_4. The current densities of Pt nanostructure deposition: (*a*) 0.14 mA/cm^2, (*b*) 0.7 mA/cm^2, (*c*) 3.5 mA/cm^2, (*d*) 7.0 mA/cm^2, and (*e*) Pt/C. The polarization potential was 0.6 V.

The EAs of all 3DPHNs were further evaluated by continuous cycling from – 0.2 V to 1.0 V in 1.0 mol/L CH_3OH + 0.5 mol/L H_2SO_4, as shown in Figure 5B. All EAs declined with the increase of cycle number, *n*. Among all samples, 3DPHNs obtained at the current density of 3.5 mA/cm^2 exhibited the best stability after 700 cycles (9.7 h). The EA of the 3DPHNs declined slowly with the increase of the cycle number, *n,* and remained at 58% of the initial value. The EAs of 3DPHNs obtained at the current densities of 0.14 mA/cm^2 and 0.7 mA/cm^2 declined

steeply to 20% and 25% of the initial EAs, respectively, after 350 cycles and remained almost steady from 350 to 700 cycles. The EA of 3DPHN obtained at the current density of 7.0 mA/cm^2 decreased to 30% of the initial value after 450 cycles and remained steady from 350 to 700 cycles. It indicated that 3DPHNs obtained at 3.5 mA/cm^2 had the best EA stability, which was better than the commercial Pt/C catalyst (47% retention of EA, curve *e*).

All 3DPHNs and commercial Pt/C were further polarized at 0.6 V for 4000 s in 1.0 mol/L CH_3OH + 0.5 mol/L H_2SO_4 solution, as shown in Figure 6. At 4000 s, 3DPHN obtained at 3.5 mA/cm^2 still exhibited the best performance among all as-prepared samples, having a longer-term stability than Pt/C, which is consistent with the cyclic voltammetric characterization in Figure 5B, and the catalytic activity was calculated to be ~ 2 times better than commercial Pt/C catalyst according to the catalytic current density, and 4.5 times better than Pt honeycomb structure.[33]

Exposed specific facets and structural morphologies of Pt catalysts are closely related to Pt electrocatalytic activity. The {111} facet is one of the most stable planes among all facets of Pt. The richness of {111} facets in the surface of 3DPNHs is one main aspect contributing to the enhanced long-term stability, as confirmed by Pt nanotubes dominated by {111} facets.[23] Previous work has found that Pt nanoparticles with {111} orientation are generally more CO tolerant than Pt nanoparticles with {100} orientation.[48] Pt octahedron enclosed by {111} facets were also demonstrated to provide more active sites than the ordinary particle surface, exhibiting an enhanced catalytic activity in methanol electrooxidation.[49] However, exposure of the {111} facets cannot be the only reason for the improvement of Pt catalytic activity. Many Pt nanostructures, such as dendritic Pt speheres,[50] and hollow Pt nanostructures[51] showed lower electrocatalytic activities in cycle voltammetric measurements than that obtained in our case (~ 1.2 mA·cm^{-2}, Figure 5A) although spikes of dendritic Pt spheres and nanoparticles of hollow Pt nanostructures had {111} orientation. The morphology of Pt nanostructures cannot be neglected because it directly affects mass transport of methanol.[51,52] For example, porous Pt meso-flowers with {111} orientation nanopedals[53] and three-dimensional dendritic Pt nanostructures composed of {111} orientation nanoparticles[40] exhibited excellent electrocatalytic activities that were 2-3 times better than that of commercial Pt/C due to improvement of methanol mass transport in catalysts.

The catalytic activities of 3DPHNs obtained at 0.7 and 7.0 mA/cm^2 were different from that of 3DPHN prepared at 3.5 mA/cm^2, the reason of which may be attributed to the difference of exposed facets, as demonstrated in Figure 2. This satisfactory catalytic activity and stability of 3DPHN obtained at 3.5 mA/cm^2 should be attributed to the exposure of {111} facets and structural morphology. The loss of catalyst may be due to surface structure rearrangement during the electrochemical cycle and the poisoning of CO-like intermediates.

4 Conclusion

One-step galvanostatic electrodeposition was demonstrated as a simple approach to fabricate three-dimensional Pt hierarchical structures consisting of nano-petals. By controlling the current density of deposition, the morphologies of 3DPHNs were adjustable and transformed from isolated nano-petal microspheres into 3D dense nano-petal arrays. Additionally, 3DPHN obtained at the current density of 3.5 mA/cm^2 has better electrocatalytic activity and stability than the commercial Pt/C catalyst in a long-term run of methanol oxidation, which was attributed to the richness of Pt{111} facets and the special morphology of 3DPHN.

Acknowledgements

This study was financed by NSFC (No. 21176060) and Chemical Science Base (Nos. J1210040 and J1103312) of Hunan University.

Notes and references

State Key Lab of Chemo/Biosensing and Chemometrics, School of Chemistry and Chemical Engineering, Hunan University, Changsha 410082, China. E-mail: liyje@hnu.edu.cn

1 Y. Wu, S. Cai, D. Wang, W. He and Y. Li, *Journal of the American Chemical Society*, 2012, 134, 8975.
2 P. Granger and V.I. Parvulescu, *Chemical Reviews*, 2011, 111, 3155.
3 S. Guo and E. Wang, *Accounts of Chemical Research*, 2011, 44, 491.
4 Y. Liu, D. Li, V.R. Stamenkovic, S. Soled, J.D. Henao and S. Sun, *ACS Catalysis*, 2011, 1, 1719.
5 Q.-S. Chen, Z.-Y. Zhou, F.J. Vidal-Iglesias, J. Solla-Gullón, J.M. Feliu and S.-G. Sun, *Journal of the American Chemical Society*, 2011, 133, 12930.
6 H. Zhang, Y. Yin, Y. Hu, C. Li, P. Wu, S. Wei and C. Cai, *The Journal of Physical Chemistry C*, 2010, 114, 11861.
7 L. Wang and Y. Yamauchi, *Chemistry of Materials*, 2011, 23 2457.
8 M.-Y. Duana, R. Liang, N. Tian, Y.-J. Li and E.S. Yeung, *Electrochimica Acta*, 2013, 87, 432.
9 H. Yang, J. Zhang, K. Sun, S. Zou and J. Fang, *Angewandte Chemie International Edition*, 2010, 49, 6848.
10 V.R. Stamenkovic, B. Fowler, B.S. Mun, G. Wang, P.N. Ross, C.A. Lucas and N.M. Marković, *Science*, 2007, 315, 493.
11 J. Suntivich, Z. Xu, C.E. Carlton, J. Kim, B. Han, S.W. Lee, N. Bonnet, N. Marzari, L.F. Allard, H.A. Gasteiger, K. Hamad-Schifferli and Y. Shao-Horn, *Journal of the American Chemical Society*, 2013, 135, 7985.
12 B.Y. Xia, H.B. Wu, X. Wang and X.W. Lou, *Journal of the American Chemical Society*, 2012, 134, 13934.
13 Y. Kang, L. Qi, M. Li, R.E. Diaz, D. Su, R.R. Adzic, E. Stach, J. Li and C.B. Murray, *ACS Nano*, 2012, 6, 2818.
14 N.S. Porter, H. Wu, Z. Quan and J. Fang, *Accounts of Chemical Research*, 2013, 46, 1867.
15 V. Komanicky, H. Iddir, K.-C. Chang, A. Menzel, G. Karapetrov, D. Hennessy, P. Zapol and H. You, *Journal of the American Chemical Society*, 2009, 131, 5732.
16 T.H.M. Housmans, A.H. Wonders and M.T.M. Koper, *The Journal of Physical Chemistry B*, 2006, 110, 10021.
17 Y.X. Chen, A. Miki, S. Ye, H. Sakai and M. Osawa, Formate, *Journal of the American Chemical Society*, 2003, 125, 3680.
18 T. Iwasita, *Electrochimica Acta*, 2002, 47, 3663.
19 E. Herrero, K. Franaszczuk and A. Wieckowski, *The Journal of Physical Chemistry*, 1994, 98, 5074.
20 X. Huang, Z. Zhao, J. Fan, Y. Tan and N. Zheng, *Journal of the American Chemical Society*, 2011, 133, 4718.
21 B.Y. Xia, H.B. Wu, Y. Yan, X.W. Lou and X. Wang, *Journal of the American Chemical Society*, 2013, 135, 9480.
22 L. Yang, X. Song, M. Qi, L. Xia and M. Jin, *Journal of Materials Chemistry A*, 2013, 1, 7316.
23 S. Ci, J. Zou, G. Zeng, S. Luo and Z. Wen, J*ournal of Materials Chemistry*, 2012, 22, 16732.

24 T. Yu, D.Y. Kim, H. Zhang and Y. Xia, *Angewandte Chemie International Edition*, 2011, 50, 2773.
25 Z.-C. Zhang, J.-F. Hui, Z.-C. Liu, X. Zhang, J. Zhuang and X. Wang, *Langmuir*, 2012, 28, 14845.
26 T. Kijima, Y. Nagatomo, H. Takemoto, M. Uota, D. Fujikawa, Y. Sekiya, T. Kishishita, M. Shimoda, T. Yoshimura, H. Kawasaki and G. Sakai, *Advanced Functional Materials*, 2009, 19, 545.
27 L.-M. Lacroix, C. Gatel, R. Arenal, C. Garcia, S. Lachaize, T. Blon, B. Warot-Fonrose, E. Snoeck, B. Chaudret and G. Viau, *ngewandte Chemie International Edition*, 2012, 51, 4690.
28 J. Yin, J. Wang, M. Li, C. Jin and T. Zhang, *Chemistry of Materials*, 2012, 24, 2645.
29 Y.-M. Fang, Z.-B. Lin, Y.-M. Zeng, W.-K. Chen, G.-N. Chen, J.-J. Sun, B. Ren and Z.-Q. Tian, *Chemistry – A European Journal*, 2010, 16, 6766.
30 Z. Peng, H. You, J. Wu and H. Yang, *Nano Letters*, 2010, 10, 1492.
31 X. Zhang, W. Lu, J. Da, H. Wang, D. Zhao and P.A. Webley, *Chemical Communications*, 2009, 195.
32 H. Zhang, F. Jiang, R. Zhou, Y. Du, P. Yang, C. Wang and J. Xu, *International Journal of Hydrogen Energy*, 2011, 36, 15052.
33 A. Ott, L.A. Jones and S.K. Bhargava, *Electrochemistry Communications*, 2011, 13, 1248.
34 J. Liu, C. Zhong, X. Du, Y. Wu, P. Xu, J. Liu and W. Hu, *Electrochimica Acta*, 2013, 100, 164.
35 Y.-B. He, G.-R. Li, Z.-L. Wang, Y.-N. Ou and Y.-X. Tong, *The Journal of Physical Chemistry C*, 2010, 114 , 19175.
36 H. Zhang, W. Zhou, Y. Du, P. Yang and C. Wang, *Electrochemistry Communications*, 2010, 12, 882.
37 I.J. Hsu, D.V. Esposito, E.G. Mahoney, A. Black and J.G. Chen, *Journal of Power Sources*, 2011, 196, 8307.
38 N. Tian, Z.-Y. Zhou, S.-G. Sun, Y. Ding and Z.L. Wang, *Science*, 2007, 316, 732.
39 H. Li, Y.-J. Li, L.-L. Sun and X.-L. Zhao, *Electrochimica Acta*, 2013, 108, 74.
40 Q. Shen, L. Jiang, H. Zhang, Q. Min, W. Hou and J.-J. Zhu, *The Journal of Physical Chemistry C*, 2008, 112, 16385.
41 H. Sun, Y. Yu, X. Li, W. Lia, F. Li, B. Liu and X. Zhang, *Journal of Crystal Growth*, 2007, 307, 472.
42 L. Zhang, D. Chen, Z. Jiang, J. Zhang, S. Xie, Q. Kuang, Z. Xie, and L. Zheng, Nano Research, 2012, 5, 181.
43 H. Sun, X. Li, Y. Chen, W. Li, F. Li,B. Liu and X. Zhang, *Nanotechnology*, 2008, 19,225601.
44 L.-X. Ding, A.-L. Wang, G.-R. Li, Z.-Q. Liu, W.-X. Zhao, C.-Y. Su and Y.-X. Tong, *Journal of the American Chemical Society*, 2012, 134, 5730.
45 J.N. Tiwari, F.-M. Pan and K.-L. Lin, *New Journal of Chemistry*, 2009, 33, 1482.
46 H. Zhao, C. Yu, H. You, S. Yang, Y. Guo, B. Ding and X. Song, *Journal of Materials Chemistry*, 2012, 22, 4780.
47 N.T. Khi, J. Yoon, H. Baik, S. Lee, D.J. Ahn, S.J. Kwon and K. Lee, *CrystEngComm*, 2014, 16, 8312.
48 J. Solla-Gullon, F.J. Vidal-Iglesias, A. Lopez-Cudero, E. Garnier, J.M. Feliu, A.Aldaz, *Physical Chemistry Chemical Physics*, 2008, 10, 3689.
49 Y. Liu, Y. Wang, J. Zhang, S. Shi, P. Feng and T. Wang, *Catalysis Communications*, 2009, 10, 1244.
50 I.J. Hsu, D.V. Esposito, E.G. Mahoney, A. Black and J.G. Chen, *Journal of Power Sources*, 2011, 196, 8307.
51 F. Bai, Z. Sun, H. Wu, R.E. Haddad, X. Xiao and H. Fan, *Nano Letter*, 2011, 11, 3759.
52 C. Hu, X. He and C. Xia, Journal of Power Sources, 2010, 195 1594.
53 L. Zhuang, W. Wang, F. Hong, S. Yang, H. You, J. Fang and B. Ding, *Journal of Solid State Chemistry*, 2012, 191 , 239.